Full Paper

Propellants, Explosives, Pyrotechnics

DOI: 10.1002/prep.201600036

Compressive Behavior of Idealized Granules for the Simulation of Composition C-4

Melissa L. Sweat,[a] Andrew S. Parker,[a] and Stephen P. Beaudoin*[a]

Abstract: In the most common approach to detect trace explosives at security checkpoints, any illicit residues must first be removed from the surface of interest (contact sampling) before they are delivered to a detector, such as an ion mobility spectrometer. Contact sampling involves applying a compressive shearing load to dislodge the residue from a surface. Optimizing this step requires an understanding of the properties of the residues and their effect on residue behavior. This study seeks to evaluate the previously unstudied effect of the binder mechanical properties and particle size distributions on the behavior of Composition C-4. Composition C-4 demonstrates complex granular behavior, and contains a highly viscous, non-Newtonian binder. In addition to studies of real C-4, simulated C-4 was created with mechanical properties very similar to the real composite. The results with the live and simulated C-4 indicate that – while highly important – the binder is not the only driving parameter controlling granule deformation under load; to create an effective simulant the binder must be combined with particles of an appropriate bimodal particle size distribution.

Keywords: Mechanical properties · Composition C-4 · Granulation · Compressive behavior

1 Introduction

The creation of a benign analog to live Composition C-4 is of interest for several key reasons. From a research perspective, an inert simulant would allow far easier access to study the mechanical behavior of C-4 without the requirement of having live explosives on site. From a checkpoint security perspective, the ability to effectively recognize threats based on contact sampling relies on the ability to remove energetic residues from a person's hands, luggage, shipping containers, or other surfaces of interest. Typically, this is done via swiping an interrogating cloth across one of these surfaces of interest to harvest residue (contact sampling). Once the sampling is complete, the swab is fed to an ion mobility spectrometer (IMS) to evaluate the presence of explosive residue. Accordingly, a key aspect of the development of improved swabs and swabbing protocols for explosives detection involves understanding the mechanisms of adhesive/cohesive failure within the energetic residue as it is removed from a surface.

Composition C-4 is comprised of 91% cyclotrimethylenetrinitramine (RDX) with 9% polymeric binder. Current military specifications for RDX list ranges of particle diameters from $<44\ \mu m$ to $<2000\ \mu m$ [1,2]. Due in part to this wide range of particle diameters, variability exists regarding the size of particles encountered in C-4 during swipe sampling [3–7]. Notably, the size of particles deposited by a thumbprint on a surface of interest has not been fully evaluated, and the ability to recreate a standard print is also lacking [3–7].

Robust trace explosives sampling techniques also have yet to be firmly established [3]. For IMS, certain standards apply: a swab must effectively remove solid particulates from a surface, withstand temperatures up to 300 °C as employed by the IMS, and be affordable [3,4]. Most current studies consider either cloth or Teflon-coated fiberglass swabs [3–7]. A number of parameters have not been successfully controlled during the development of an optimal wiping technique [6]. Variability exists in the applied force during swiping, the surface area covered, the swab material, the roughness of the swab and substrate materials, the swipe velocity, and the number of times a swab may be reused before it is discarded [3,6,7]. Studies by Verkouteren et al. claim that the critical parameters in determining removal efficiency are applied load and the translational force required to overcome the frictional resistance at the swipe-substrate interface to maintain a constant swiping velocity [3]. They also note a direct linear correlation between increased applied force of swiping and particle removal efficiency [3,5,6]. While Verkouteren et al. indicate a swipe speed of $0.7\ cm\,s^{-1}$ in their studies, the Environmental Protection Agency indicates swipe sampling speeds

[a] *M. L. Sweat, A. S. Parker, S. P. Beaudoin*
School of Chemical Engineering
Purdue University
480 Stadium Mall Drive
West Lafayette, IN 47907 – 2100 USA
**e-mail: sbeaudoi@purdue.edu*

of 10 and 17 cm s^{-1} in its work [3,8]. Note that the speed of a swipe directly correlates to the strain rate, and thus the viscosity of the non-Newtonian binder in the residue, as non-Newtonian fluids have strain-dependent viscosity. All of these parameters require investigation to more fully understand the nature of swipe testing and improve trace explosives detection at security checkpoints.

A major challenge to the development of improved swipes and swiping protocols lies in the creation of a benign analog to live explosive materials, such as C-4. The creation of such a material serves two primary functions: the ability to conduct mechanical properties tests on inert C-4 eliminates the necessity of having any quantity of detonable material present, increasing the safety of the tests. Additionally, the ability to recreate C-4 using benign ingredients allows significant insight into the primary factors controlling its mechanical behavior, which is the main focus of this study.

2 Experimental

2.1 Materials

Three powders were used to create granular material in this study: >230 mesh silica, 40–150 mesh silica, and 30–40 mesh silica (Figure 1). Particle characteristics for each of these powders are given in Table 1, including the surface weighted mean (Sauter mean diameter, x_{32}), the 10th percentile diameter (x_{10}), the median diameter (x_{50}), the 90th percentile diameter (x_{90}), and the particle circularity. These particles were chosen based on their relative similarity to the RDX size distribution used in the preparation of live C-4 [9]. The circularity (C) is calculated by Equation (1), where the area (A_p) and perimeter (P) of the particles is easily obtained through image processing software [10]. Though the circularities presented herein appear to be similar, this is not the case: the highly irregular powder lactose has a circularity of 0.72, while largely uniform, spherical glass beads often have circularities of 0.9–0.95 [11].

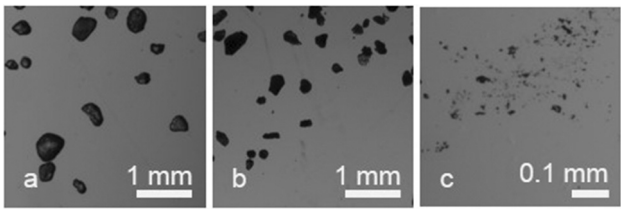

Figure 1. Optical microscopy image of the 30–40 mesh silica (a), 40–150 mesh silica (b), and >230 mesh silica (c) powders [12].

$$C = 4\pi \frac{A_p}{P^2} \quad (1)$$

The cumulative particle size distributions as evaluated by a Malvern Mastersizer 200 Light Diffraction Particle Size Analyzer are given in Figure 2. These particles were chosen based on their relative similarities to the powder sizes of RDX used in the creation of Composition C-4 (Table 2)

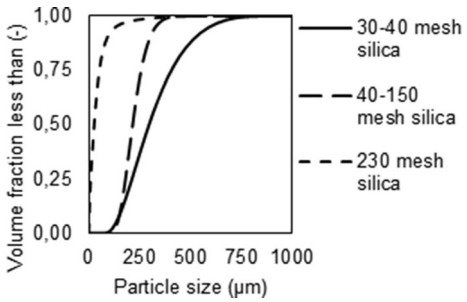

Figure 2. Cumulative particle size distributions for 30–40 mesh silica, 40–150 mesh silica, and >230 mesh silica powders [12].

Table 2. RDX size distribution for use with Composition C-4 [1,2].

U.S. Standard Sieve No.	Particle size [μm]	Coarse [%]	Fine [%]
325	44	n/a	97
200	74	18	n/a
100	149	35	n/a
50	300	90	n/a
20	841	98	n/a

[1,2]. With respect to the size distributions of "Coarse" and "Fine" RDX shown, the designations provided indicate the cumulative distribution of particles fitting through the given sieves size: the #100 sieves size represents the particles that are larger than 149 μm, including those that fall through the #20 and #50 sieves. For the first part of this study, granules were prepared with unimodal size distributions as depicted in Figure 2. Additional studies were conducted on granules prepared with a bimodal size distribution, with cumulative and frequency size distributions as given in Figure 3 and Figure 4. For this study, when the bimodal size distribution is referenced, the first number in

Table 1. Particle size characteristics for all silica powders shown in Figure 1 [12].

Sample	x_{32} [μm]	x_{10} [μm]	x_{50} [μm]	x_{90} [μm]	Circularity
30–40 mesh	279 ± 36	155 ± 06	312 ± 37	547 ± 0.28	0.81 ± 0.06
40–150 mesh	208 ± 07	155 ± 06	215 ± 07	300 ± 09	0.75 ± 0.08
>230 mesh	4 ± 03	3 ± 01	27 ± 06	95 ± 42	0.67 ± 0.18

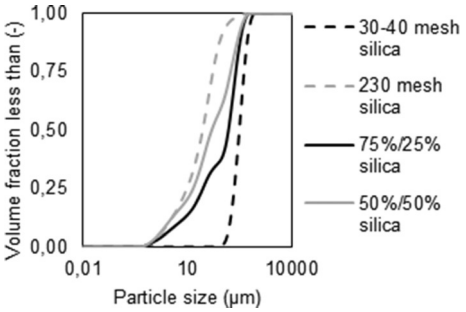

Figure 3. Cumulative particle size distributions for the powders used in granule creation. For the bimodal distributions, the first percentage refers to the mass fraction of 30–40 mesh silica, and the second percentage represents the mass fraction of the >230 mesh silica [12].

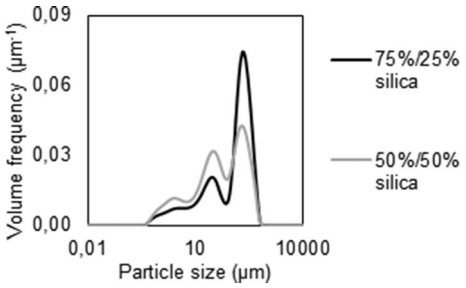

Figure 4. Frequency particle size distributions for the bimodal powders in this study. For the bimodal distributions, the first percentage refers to the mass fraction of 30–40 mesh silica, and the second percentage represents the mass fraction of the >230 mesh silica [12].

a percentage (e.g., the 75% in the 75%/25% mixture) represents the mass fraction of 30–40 mesh silica included in the mixture. The second value (25%, in this example) is the amount of >230 mesh silica included.

Three types of granules were considered in this study: live C-4, ideal granules (particles bound with polydimethylsiloxane (PDMS) of varying viscosity), or simulated C-4 (comprised of 91 wt-% particles with 9 wt-% simulated C-4 binder. The viscosities of the PDMS (a Newtonian fluid) were 12, 29, 58, 97, 289, 579, 965, and 2413 Pa s. The simulated C-4 binder consisted of 59 wt-% bis(2-ethylhexyl) sebacate, 23 wt-% polyisobutylene, and 18 wt-% SAE 10 nondetergent motor oil, per the standard recipe [13]. The resulting highly viscous, non-Newtonian binder was evaluated using a TA Instruments rotational rheometer. Based on Figure 5, the binder is shear-thinning, indicating that the viscosity decreases as increased shear is applied, as might be expected with increased downward applied force or an increase to swipe velocity in contact sampling protocols.

2.2 Methods

Three types of granules were prepared: live C-4, simulated C-4, and ideal. The live C-4 granules were provided in accordance with the military specifications for the explosive material. The simulated C-4 was prepared with simulated C-4 binder (9 wt-%) mixed with 91 wt-% particles; the particles used were one of the two unimodal distributions (40–150 mesh silica, or 30–40 mesh silica) or one of the two bimodal distributions (75% 30–40 mesh silica mixed with 25% >230 mesh silica or 50% each 30–40 mesh silica and >230 mesh silica). The ideal granules were prepared with PDMS and 40–150 mesh silica. The ideal granules and the simulated C-4 composites were prepared by hand and care was taken to ensure thorough and uniform mixing. Each granule was compressed into a cylindrical mould to form a granule with a diameter of 25 mm. The height of each granule was approximately 25 mm; the precise height was determined experimentally.

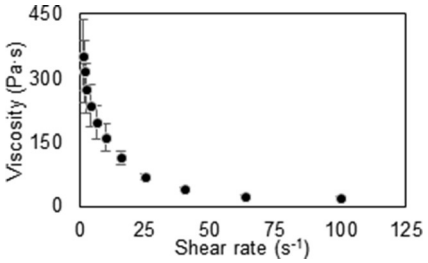

Figure 5. Viscosity of simulated C-4 binder as a function of applied shear rate [14].

The compression experiments performed in this study were similar to those described elsewhere [12, 14–17]. Each granule was placed on the lower platen of an Instron ElectroPuls E1000. To minimize frictional effects, both the upper and lower platen were lubricated. Granules were compressed in both axial (cylindrical face perpendicular to the direction of compression) and diametrical (cylindrical face parallel to the direction of compression) orientations at compression rates of 1, 10, and 100 mm s^{-1}. The velocities correspond to engineering strain rates of 0.04, 0.43, and 4.65 s^{-1} according to Equation (2), where $\dot{\varepsilon}$ is the strain rate, ε is the engineering strain, t is time, h_o is the initial height of the granule, and v is the compression rate.

$$\dot{\varepsilon} = \frac{d\varepsilon}{dt} = \frac{1}{h_o}\frac{dh}{dt} = \frac{v}{h_o} \tag{2}$$

From these compression tests, the overall stress behavior as a function of strain was observed. Equation (3) and Equation (4) describe the engineering strain and stress, respectively, where h is the instantaneous height of the granule, F is the measured force, and A is the cross-sectional area of the granule assuming uniform barreling.

$$\varepsilon = \Delta h / h_o \tag{3}$$

$$\sigma = F/A \tag{4}$$

3 Results and Discussion

3.1 Typical Compression Results

Figure 6 shows a stress-strain curve typical of a granular compression experiment. The solid line represents the average stress-strain curve from 5–10 replicates, and the dotted lines are one standard deviation from the mean. There are four main sections of this curve (labeled a–d) with corresponding images found in Figure 7. The images on the top (1a–1d) of Figure 7 correspond to the axial orientation, and the bottom images (2a–2d) depict granules in the diametrical orientation. The first set of images (a) depicts granules immediately following placement on the lower platen – before any compression occurred. The second set of images (b) is representative of the granule at the peak flow stress. This was the maximum stress observed throughout the experiment. Approximately halfway between the peak flow stress and $\varepsilon = 0.5$, the granule presented significant deformation (c). The test concluded at $\varepsilon = 0.4$, represented by the final images (d). In general, between conditions (c) and (d), a marginal increase to the stress was observed due to granular barreling. As the compression progressed, some material was forced outward. At a point $\varepsilon \approx 0.4$, this "external" barreling began to form walls surrounding the "inner" granule. This resulted in a stress increase as the compression transitioned from unconfined compression to confined compression.

The images presented in Figure 7 are representative of all results generated in this work – no observable "failure" of the granule occurred. Through the peak flow stress (b), only very minimal deformation has occurred. Major deformation did not occur until over halfway through the test. Even at high strain ($\varepsilon > 0.3$), no plane of failure was observed. Some void creation was noted at the exterior of the granule, though these voids are quite shallow, only extending 2–3 mm into the bulk material. Finally, following the conclusion of the compression, the granules were typically removed as one solid piece, indicating that the material did not fail. Instead, only significant deformation occurred.

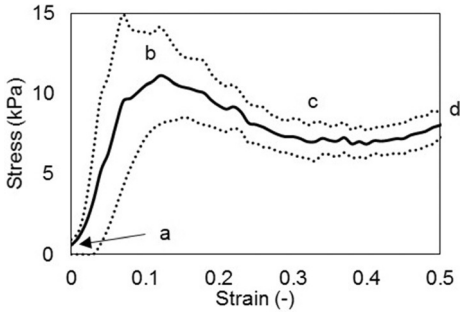

Figure 6. Representative experimental result for compression tests. The solid line is the average result, and the dotted lines represent the standard deviation from the average. Letters a–d correspond to the images shown in Figure 7. This particular test is for granules comprised of 30–40 mesh silica particles in simulated C-4 binder compressed at 10 mm s^{-1} ($\dot{\varepsilon} = 0.43 \pm 0.08$ s^{-1}).

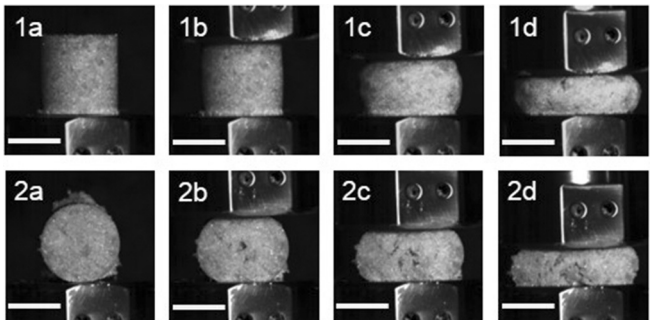

Figure 7. Images corresponding to the stress-strain curve presented in Figure 6. (1) and (2) designations refer to the axial and diametrical configurations, respectively. The images at (a) are the initial shapes prior to any applied stress. The peak flow stress is reached at (b). (c) indicates a point approximately halfway between the peak flow stress and strain = 0.5, and the images at (d) correspond to strain = 0.5. The scale bar is 1 cm.

3.2 Live C-4

Compression tests were completed using live C-4 at 1, 10, and 100 mm s^{-1} compression rates, with results as shown in Figure 8. Note that the solid line indicates the average stress-strain curve from 5–10 replicates, while the shaded regions represent the standard deviation from the mean. The most notable effect resulted from the change in strain rate: as strain rate increased, granular strength also increased, though this effect is small between the 1 and 10 mm s^{-1} compression rates. The general trends observed were consistent with those shown in Figure 6 – a sharp rise in stress occurred at $\varepsilon < 0.2$, after which the stress was reduced to a minimum followed by a secondary increase resulting from barreling.

An increase in peak flow stress resulting from increased strain rate has been observed for polymeric materials. The ratio of relaxation time to observation time is commonly

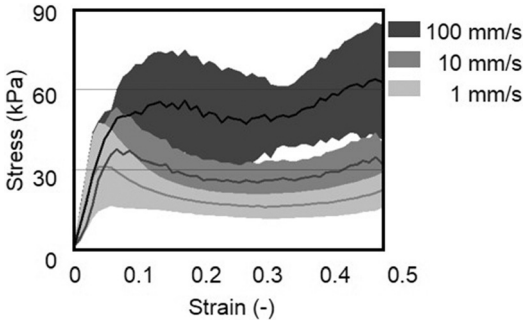

Figure 8. Stress-strain behavior of live C-4 during compression experiments at 1, 10, and 100 mm s^{-1} compression rate. The solid lines represent the average at each binder viscosity, and the shaded regions correspond to one standard deviation from the mean [14].

used to describe this phenomenon [18]. If the relaxation time is significantly shorter than the observation time, then the material will flow. Conversely, if the observation time is significantly shorter than the relaxation time, the material will not have enough time to relax, and no flow will be observed. For the compression experiments conducted here, increasing strain rate results in a decrease to observation time. However, the relaxation time for a given binder remains constant. As such, the binder had less time to react to an applied strain, and maintaining constant compressive velocity caused an increase to the granular stress. This is observed in Figure 8 (and all remaining compression tests), where the lowest strain rates allow the material to flow more readily than at higher strain rates.

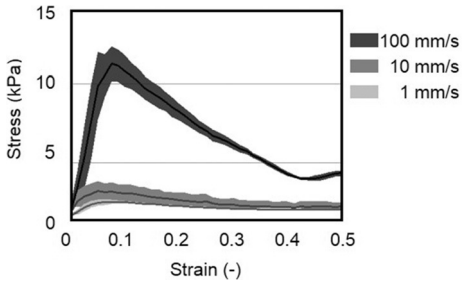

Figure 10. Stress-strain results from compression experiments for ideal granules prepared with 29 Pa s PDMS binder at 10 mm s^{-1} compression rate. The solid lines represent the average at each binder viscosity, and the shaded regions correspond to one standard deviation from the mean.

3.3 Simulated C-4

3.3.1 Effects of the Binder

Compression experiments were conducted on the aforementioned granules prepared with simulated C-4 binder and 40–150 mesh silica powder. Figure 9 shows these results for granules compressed at 1, 10, and 100 mm s^{-1}. The general shapes and trends observed are remarkably similar to those for the live material, though the magnitude of the granular strength is greatly reduced. This is expected, as the simulated material here was prepared with a unimodal distribution, and the live C-4 contains a bimodal distribution of RDX. The increased packing fraction present in the live C-4 is likely to resist motion more effectively than in the simulated material, creating a stronger granule. This will be further explored in sections 3.3.3 and 3.3.4. For comparison, ideal granules prepared with 40–150 mesh silica and 29 Pa s PDMS compressed at 1, 10, and 100 mm s^{-1} are shown in Figure 10. From these figures, a major difference in the granular behavior is immediately observed: the variation in observed stress responses is far greater in the simulated and live C-4 than in the ideal granules, as will be discussed in greater detail in the following section.

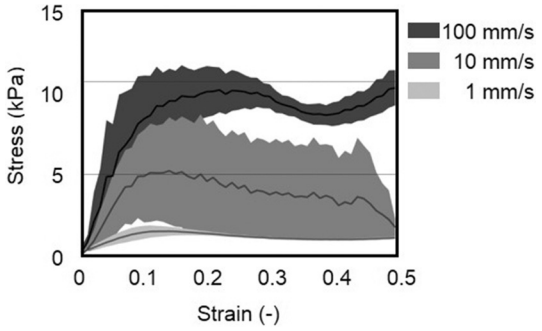

Figure 9. Stress-strain results from compression experiments for simulated C-4 at 1, 10, and 100 mm s^{-1} compression rate. The solid lines represent the average at each binder viscosity, and the shaded regions correspond to one standard deviation from the mean.

3.3.2 Discussion of Binder Effects

A comparison of the peak flow stress data for all of the granules studied is shown in Figure 11. Based on Equation (1), the strain rates for 1, 10, and 100 mm s^{-1} compression rates are 0.04, 0.43 and 4.65 s^{-1}, respectively. Based on the peak flow stress data, the simulated C-4 was most similar to ideal granules created with low viscosity PDMS (Newtonian binders). In addition, none of the simulated C-4 (either with a simulated C-4 binder or with PDMS binders) showed peak flow stress behavior that matched that of live C-4 over all three strain rates. When a load was applied to the granules, it was assumed that particles within the granule moved relative to each other at different rates depending on their location within the granule. Since the C-4 binder is non-Newtonian, this means that the local binder viscosity varied throughout the granule. In addition, because the local particle velocities were expected to change over the course of a compression experiment, the local viscosity was expected to change with time as well.

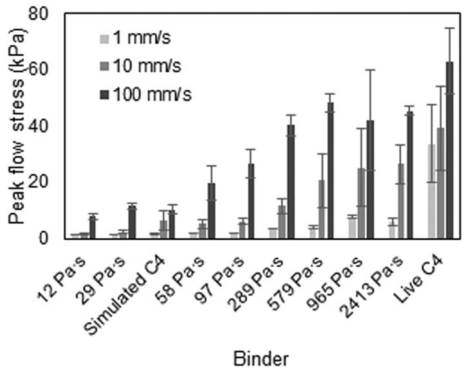

Figure 11. Peak flow stress as a function of increasing compression rate for simulated C-4 prepared with 40–150 mesh silica compared with granules created with 40–150 mesh silica and PDMS and live C-4. Note that 1, 10, and 100 mm s^{-1} correspond to strain rates 0.042 ± 0.004, 0.431 ± 0.076, and 4.651 ± 1.752 s^{-1}, respectively.

To further confirm the importance of using a representative non-Newtonian binder in the creation of a benign analog, simulated and live C-4 granules were compared with granules prepared with PDMS, as shown in Figure 11. Based solely on this image, if one were to compare the peak flow stress value (in the absence of any other curve feature), the simulated C-4 granule would exhibit behavior most closely associated with that seen in the PDMS-containing granule containing PDMS of viscosity ca. 30 Pa s. However, this is misleading for two reasons: first, the overall curve behavior demonstrated by the ideal composite (PDMS with silica particles) is clearly not representative of the simulated or live composites (Figure 8, Figure 9, and Figure 10). Second, based on the viscous profile of the C-4 binder, a viscosity of only 30 Pa s is unrealistically low for the shear rates that might be expected for the compression rates examined here. This confirms that the rheology of the non-Newtonian binder is highly important to creating a benign simulant that mimics the mechanical behavior of live C-4.

This phenomenon also explains the distinct trends observed surrounding the peak flow stress behavior exhibited in Figure 8, Figure 9, and Figure 10. The applied force was distributed in a non-uniform manner throughout each granule as a result of the particle distribution within the granule. As particles experienced increased strain, any non-Newtonian binder directly in contact with the particles underwent a decrease in viscosity. However, binder surrounding particles not experiencing strain maintained a very high viscosity by comparison. These regions of low viscosity potentially lubricated the regions of high viscosity, further increasing the complexity of the system. Such behavior could not occur when Newtonian binders are applied. As a result, ideal granular materials prepared with Newtonian binders cannot respond to an applied strain, as occurs during swiping, in the same manner as live C-4 or simulated C-4 which has a realistic (non-Newtonian) binder. The creation of a benign analog to live C-4 must incorporate a similarly non-Newtonian binder. When a non-Newtonian binder with similar flow properties as the real C-4 is applied, the mechanical behaviors of the different materials under load were similar qualitatively, but lacked a strong quantitative correlation. This is likely due to one of two effects: (a) a powder with a monomodal size distribution was used to create the synthetic C-4 used here, while live C-4 contains RDX particles with a bimodal size distribution; or (b) the mechanical or surface properties of the powder used in these synthetic granules (silica) are different from those of the RDX found in the live C-4. The effects of particle size distribution – especially as impacting the magnitude of the peak flow stress – are discussed in the following sections.

3.3.3 Effects of Unimodal Size Distribution

Compression experiments were conducted on granules made from the previously mentioned small (40–150 mesh) and large (30–40 mesh) unimodal powders compounded with simulated C-4 binder. Figure 12 shows the results for simulated C-4 prepared with 30–40 mesh silica particles. The general shapes and trends observed are remarkably similar to those for the live material. Additionally, results are shown in Figure 13 for simulated C-4 prepared with each of the two different unimodal powders at 10 mm s^{-1} compression rate. While some distinctions may be made between granules prepared with the different powders, both generally follow the trend previously described (a rise in stress to a maximum, after which the stress was reduced to a minimum followed by a secondary increase resulting from barreling). Figure 14 compares the peak flow stresses of the simulated granules prepared with unimodal particle size distributions with those from the live C-4. As previously indicated, all granules show a general trend of increasing stress with increasing strain rate.

As shown in Figure 13 and Figure 14, the larger silica size fraction produces granules that are stronger than the smaller size fraction. This is contrary to many previous granulation studies, which indicate that smaller particles will result

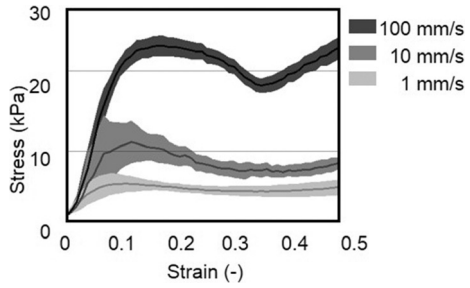

Figure 12. Stress-strain results from compression experiments at 1, 10, and 100 mm s^{-1} compression rate for simulated C-4 granules containing 30–40 mesh (unimodal) silica particles mixed with C-4 binder. The solid lines represent the average stress-strain curve, and the shaded regions correspond to one standard deviation from the mean.

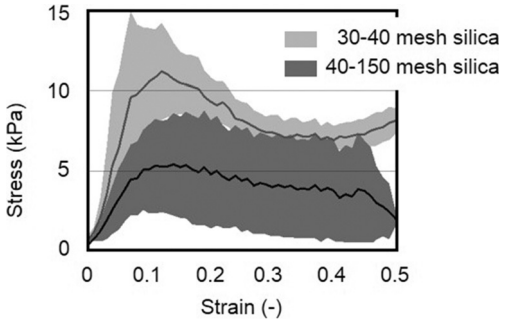

Figure 13. Stress-strain results from compression experiments at 10 mm s^{-1} compression rate for simulated C-4 granules containing unimodal powders of 40–150 mesh or 30–40 mesh particles compounded with simulated C-4 binder. The solid lines represent the average stress-strain curve, and the shaded regions correspond to one standard deviation from the mean.

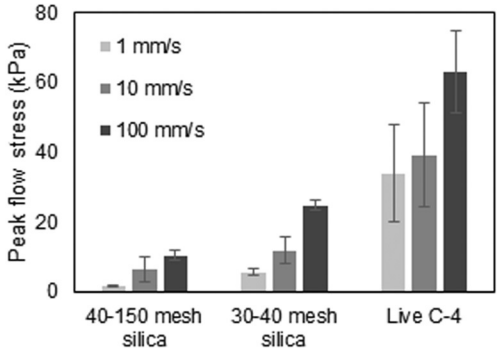

Figure 14. Peak flow stress as a function of compression rate for simulated and live C-4. Note that 1, 10, and 100 mm s^{-1} correspond to strain rates 0.042 ± 0.004, 0.431 ± 0.076, and 4.651 ± 1.752 s^{-1}, respectively.

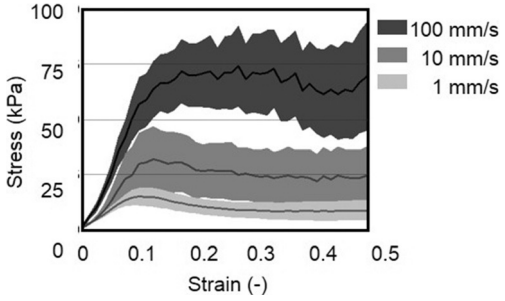

Figure 15. Stress-strain results from compression experiments with 75% 30–40 mesh and 25% > 230 mesh (bimodal) silica at 1, 10, and 100 mm s^{-1} compression rates with simulated C-4 binder. The solid lines represent the average stress-strain curve, and the shaded regions correspond to one standard deviation from the mean.

in an increase to granular strength due to the increased number of interparticle contacts per unit volume [11, 16, 19–22]. However, these other studies considered particles that were less than 100 μm in diameter and very smooth. The particles considered here are significantly larger and significantly less uniform. Hence, the increase to granular strength may be attributed to the increasingly chaotic packing of particulates within the granule – more uniform particles require more force before granular deformation may occur due to the more ordered packing.

A comparison of granular strength (Figure 14) reveals that – though the general trends are quite similar between the simulated and live C-4 as indicated by Figure 12 and Figure 13 – the overall granular strength is vastly different. There is some increase to peak flow stress with increasing particle size for the simulated materials; however, the peak flow stresses for the live C-4 are significantly greater than those for the simulated materials. This is likely due to the presence of a secondary size fraction in the live material (see Table 1).

3.3.4 Effects of a Bimodal Size Distribution

The previous section described the effect of particle size on granule behavior for particles with unimodal size distributions. While the overall trends are similar to that of live C-4, the magnitudes of the stresses are significantly lower for the simulated materials studied than for the live material. To account for this discrepancy, and to create a simulated granule closer in mechanical behavior to the live material, a secondary powder with a very small particle size distribution (> 230 mesh) was added to the 30–40 mesh (large) silica in two mass fractions: one with 75% large silica and 25% small silica and one with 50% each large and small silica.

Figure 15 shows the results of compression studies for granules created with 75% large silica compressed at 1, 10, and 100 mm s^{-1}. As strain rate increases, the observed stress increases in the same manner as previously observed: the highest strain rate corresponds to the largest observed stress. This is true for all granular materials studied here – unimodal, bimodal, Newtonian binders, non-Newtonian binders, and live C-4 (Figure 8, Figure 9, and Figure 10, Figure 12 and Figure 13). This increase is clearly a by-product of solid particles being mixed with a binder to create a granular material. However, the observed magnitude of the stress response is qualitatively very similar to that of live C-4.

A more quantitative comparison of the stress responses of simulated and the live C-4 is shown in Figure 16, which shows the peak flow stresses of simulated C-4 made with powder with a unimodal size distribution, simulated C-4 made with powders with a bimodal size distribution, and live C-4. All of the granules prepared with 100% 30–40 mesh silica particles are weaker than both the granules with particles having a bimodal size distribution and the live composites. At 1 mm s^{-1} compression rate, the live C-4 is still moderately stronger than the granules made with particles with a bimodal size distribution. However, there is no statistical difference between the peak flow stresses of

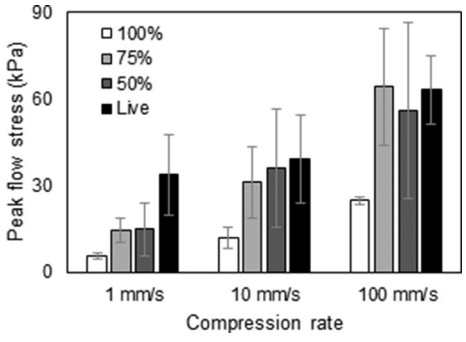

Figure 16. Peak flow stress as a function of increasing compression rate for simulated C-4 compared with live C-4. For the bimodal distributions, the percentage refers to the mass fraction of 30–40 mesh silica, with the remaining mass fraction comprised of the > 230 mesh silica. Note that 1, 10, and 100 mm s^{-1} correspond to strain rates 0.042 ± 0.004, 0.431 ± 0.076, and 4.651 ± 1.752 s^{-1}.

simulated C-4 made with particles with a bimodal size distribution and the live C-4. This suggests that a benign analogue to live C-4 may be created and that the mechanical, compressive behavior of C-4 is controlled by the particle size distribution and binder properties. Further, the implication presented herein is that the presence of a bimodal distribution is more significant than the amount of each size fraction included, over the range of fractions considered. For all compression rates, the granules prepared with 75% large silica are nearly identical to those prepared with only 50% large silica. Finally, it is important to note that while the composition of the particles compounded in the simulated C4 is quite different from that of the particles in the live C4, there is no effect of this compositional change on the mechanical properties of these materials.

4 Conclusions

The effects of binder composition and flow properties on the behavior of granules of live and simulated C-4 were considered. Additionally, the influences of particle size, particle size distribution, and particle composition on the overall behavior of simulated C-4 were examined. Simulated C-4 granules prepared with benign particles mixed with C-4 binder were observed to behave in a manner that is qualitatively similar to that of live C-4 when exposed to a compressive load. No material failure was observed in any experiments performed, and all granules were able to be removed following compression experiments in a single piece. No major plane of failure was observed for any granule. Additionally, all granules exhibited similar compressive behavior: a peak flow stress followed by a decrease in observed stress. For all granules, as strain rate increased, the observed strength of the granules universally increased, as well.

When ideal granules prepared with the same particles but with Newtonian binders of varying viscosity were tested, their mechanical response was much less similar to that of the live C-4 than that of the granules made with C-4 binder. At no point during the load testing was material observed to "fail" (as defined by the presence of a primary plane of separation preventing the removal of the material as one solid piece). Additionally, the strength of all granules was observed to increase with increasing strain rate, likely due to the decrease in observation time with respect to the characteristic relaxation time of the granules.

With respect to particle size distribution, a benign analogue to live C-4 will require a bimodal size distribution. In fact, a reasonable representation of live C-4 was created for this study using inert, silica particles with an appropriate bimodal size distribution. Combining all of the results presented in this study, the clear conclusion is that the influence of the binder coupled with the bimodal size distribution results in the characteristic compressive behavior of live C-4. Finally, if the particle size distribution is prepared correctly, and if the composition of the binder is correct, the composition of the particles is not important to the mechanical behavior of the compounded explosive.

These results are promising for future research focused on checkpoint detection of explosives by contact sampling. From a bulk perspective, the created simulant behaves in a mechanical similar manner to the explosive material. This suggests that a benign surrogate may be developed that will allow researchers to develop effective sampling methods without having to resort to experiments using live explosives. This will speed the progress of advances in checkpoint security and the development of more efficient checkpoint security methods.

Acknowledgements

This material is based upon work supported by the U.S. Department of Homeland Security, Science and Technology Directorate, Office of University Programs, under Grant Award 2013-ST-061-ED0001. The views and conclusions contained in this document are those of the authors and should not be interpreted as necessarily representing the official policies, either expressed or implied, of the U.S. Department of Homeland Security. The authors would also like to express appreciation for Mike Koppes for his assistance with the explosives materials and Osvaldo Campanella and Mine Eren for their assistance with evaluating the binder viscosity. The authors would also like to thank Alyssa Bass and Chris Browne for their assistance with this work.

References

[1] *Detail Specification: Composition C-4*, Military Specification MIL-DTL-45010B, U.S. Army Armament Research, Development, and Engineering Center, Picatinny Arsenal, NJ, USA, **2014**.
[2] *Detail Specification: RDX (Cyclotrimethylenetrinitramine)*, Military Specification MIL-DTL-398D, U.S. Army Armament Research, Development, and Engineering Center, Picatinny Arsenal, NJ, USA, **1996**.
[3] J. R. Verkouteren, J. L. Coleman, R. A. Fletcher, W. J. Smith, G. A. Klouda, G. Gillen, A Method to Determine Collection Efficiency of Particles by Swipe Sampling, *Meas. Sci. Technol.* **2008**, *19*, 115101.
[4] J. R. Verkouteren, Particle Characteristics of Trace High Explosives: RDX and PETN, *8th ISADE International Symposium on Analysis and Detection of Explosives*, Ottawa, Canada, June 6, **2004**, pp. 335–340.
[5] J. R. Verkouteren, J. L. Coleman, I. Cho, Automated Mapping of Explosives Particles in Composition C-4 Fingerprints, *9th International Symposium on the Analysis and Detections of Explosives/4th Forensic International Network for Explosives Investigation*, Paris, France, July 1–7, **2007**, pp. 334–340.
[6] J. R. Verkouteren, N. W. M. Ritchie, G. Gillen, Use of Force-Sensing Array Films to Improve Surface Wipe Sampling, *Environ. Sci. Processes Impacts* **2013**, *15*, 373–380.
[7] M. E. Staymates, J. Grandner, J. R. Verkouteren, Pressure-Sensitive Sampling Wands for Homeland Security Applications, *IEEE Sens. J.* **2013**, *13*, 4844–4850.
[8] S. Billets, *A Literature Review of Wipe Sampling Methods for Chemical Warfare Agents and Toxic Industrial Chemicals*, Report

EPA/600/R-07, National Explosure Research Laboratory: Environmental Sciences Division, Las Vegas, NV, USA, **2007**.

[9] B. T. Fedoroff, O. E. Sheffield, *Composition C Type Explosives*, in: *Encyclopedia of Explosives and Related Items*, Vol. 3, Picatinny Arsenal, NJ, USA, **1966**, pp. 485.

[10] W. S. Rasband, *ImageJ.*, US National Institute of Health, Bethesda, MD, USA, **2014**.

[11] R. M. Smith, *Wet Granule Breakage in High Shear Mixer Granulators*, PhD Thesis, University of Queensland, St. Lucia, Queensland, Australia, **2007**.

[12] M. L. Sweat, A. S. Parker, S. P. Beaudoin, Compressive Behavior of High Viscosity Granular Systems: II. Effect of Particle Size Distribution, *Powder Technol.*, submitted.

[13] *Detail Specification: Polyisobutylene Binder*, Military Specification MIL-P-14536 w/Amendment 1, U.S. Army Armament Research, Development, and Engineering Center, Picatinny Arsenal, NJ, USA, **2012**.

[14] M. L. Sweat, A. S. Parker, S. P. Beaudoin, Compressive Behavior of High Viscosity Granular Systems: I. Effects of Viscosity and Strain Rate, *Powder Technol*, **2016**, DOI: 10.1016/j.powertec.2016.06.047.

[15] R. M. Smith, J. D. Litster, Examining the Failure Modes of Wet Granular Materials using Dynamic Diametrical Compression, *Powder Technol.* **2012**, *224*, 189–195.

[16] S. M. Iveson, N. W. Page, Dynamic Strength of Liquid-Bound Granular Materials: The Effect of Particle Size and Shape, *Powder Technol.* **2005**, *152*, 79–89.

[17] S. M. Iveson, N. W. Page, Brittle to Plastic Transition in the Dynamic Mechanical Behaviour of Partially Saturated Granular Materials, *J. Appl. Mech.* **2004**, *71*, 470–475.

[18] M. Reiner, The Deborah Number, *Phys. Today* **1964**, *17*, 62.

[19] J. D. Litster, B. J. Ennis, *Consolidation, Coalescence and Growth*, in: *The Science and Engineering of Granulation Processes* (Ed.: B. Scarlett, L. Liu), Kluwer Academic Publishers, Dordrecht, **2004**, pp. 78–82.

[20] S. M. Iveson, J. A. Beathe, N. W. Page, The Dynamic Strength of Partially Saturated Powder Compacts: the Effect of Liquid Properties, *Powder Technol.* **2002**, *127*, 149–161.

[21] H. G. Kristensen, P. Holm, T. Schaefer, Mechanical Properties of Moist Agglomerates in Relation to Granulation Mechanisms Part II. Effects of Particle Size Distribution, *Powder Technol.* **1985**, *44*, 239–247.

[22] G. V. Franks, F. F. Lange, Plastic Flow of Saturated Alumina Powder Compacts: Pair Potential and Strain Rate, *AIChE J.* **1999**, *45*, 1830–1835.

Received: February 4, 2016
Revised: May 11, 2016
Published online: August 23, 2016

